2014 IEEE International Conference on Robotics & Automation (ICRA)
Hong Kong Convention and Exhibition Center
May 31 - June 7, 2014. Hong Kong, China

Design of Flexonic Mobile Node using 3D Compliant Beam for Smooth Manipulation and Structural Obstacle Avoidance

Jiajie Guo[1], *IEEE Member*, Wuguang Liu[1] and Kok-Meng Lee[1,2*] , *Fellow, IEEE*

***Abstract*—Motivated by the needs to develop dexterous flexonic mobile node (FMN) for structural health monitoring where obstacle avoidance is among the most challenging tasks, this paper presents a novel FMN design for navigating on iron-based structures. Unlike most existing magnetic wheel designs, the FMN uses fixed-magnet configuration contributing to smooth motion, self-maintained orientation and automatic negotiation of concave corners. Taking into account of several stringent considerations (including tight dimension, efficient attachment and manipulation flexibility) to facilitate avoidance of structural obstacles in tight space, a prototype FMN incorporating a compliant beam (that results in more DOFs than designs with multiple links and pin/ball joints), along with a 3-step strategy for negotiating a convex corner, has been developed. Although controlling a continuous deforming beam is challenging given limited number of actuators, both simulation and experimental results confirm a simple input/output relation between the rear axle displacement and front axle rotation, which is anticipated to facilitate control implementation of FMN for obstacle avoidance.**

I. Introduction

In recent years, wireless sensor networks have grown to be a practical and promising approach for civil structural health monitoring (SHM) [1, 2]. In a mobile sensor network, each node is a sensor-carrying robot capable of autonomous navigation and wireless communication with peers. Given the complicated civil structures (with corners, steps, reinforced ridges, etc.), a mobile robot must embody a flexible structure for negotiating various obstacles and for attaching/detaching a sensor onto/from ferromagnetic surfaces as well as perform other potential functions for SHM applications[3, 4]. Inspired by biological limbs (such as octopus tentacles and elephant trunks) that enable many animals the capabilities of dexterous locomotion and compliant manipulation, researchers have been developing flexible robots featuring compliant beams for continuous bending and twisting[5-9]. However, it is a challenging task to design and control a compliant beam subjected to nonlinear deformations with kinematic redundancy in the three-dimensional (3D) space. There is a need for an efficient method for designing flexible robots, which describes all state variables in a global coordinate while accounting for both focal and distributed loadings along the beam. This is achieved by derivation based on curvatures, which is inherent to geometry and independent of coordinate frames. For this reason, the method is named as curvature-based beam model (CBM), which is used for designing and controlling a novel robot with a flexible structure referred to here as a "flexonic mobile node" (FMN). Unlike rigid configurations with a fixed distance between the front and rear axles of a car-like robot, the FMN features various deformable configurations in the 3D space by incorporating a compliant beam (connecting the front and rear axles with a controlled pin joint) and thus enabling it to flexibly navigate on ferromagnetic structures.

It has been widely accepted that mimicking morphology of animals/insects is beneficial to the design of autonomous robots [10]. To accomplish agile and dexterous motions, researchers have to employ various types of joints and actuators, as well as complicated sensory feedback control loops. With typical actuators in mind, additional degrees of freedom (DOFs) usually require more actuators/sensors/batteries, which would result in bulky and chunky robot bodies and hence increased robot inertia with compromised agility. With elegant designs and advanced control techniques, hyper-redundant robots are fabricated as a flexible structure consists of a series of actuated joints to emulate motions of snakes [11, 12] and lampreys [13]. However, redundant designs are hard to realize on small scale. To reduce the number of actuators while maintaining the characteristic of flexibilities, researchers have been using smart materials, such as the ionic conducting polymer film (ICPF) and the ionic polymer-metal composite (IPMC) for a fish-like micro robot [14, 15]. Recently, a new medical device of active cannula comprising of super-elastic concentric tubes [16, 17] has been designed. Due to the features of continuous bending and twisting, they are also known as flexible robots. Their designs with conventional actuators and commercially available elastic materials (such as linear/rotational motors and Nitinol) have brought up the question on how to control a mechanism with continuous large deformation using very few actuator inputs. This paper intends to provide a preliminary answer to this question from the viewpoint of designing and modeling of an FMN.

Manuscript received September 15, 2013. This work was supported in part by National Basic Research Program of China (973 Program, Grant No. 2013CB035803), Fundamental Research Funds for the Central Universities (HUST: 2012QN253), and the State Key Lab of Digital Manufacturing Equipment and Technology (DMETZZ2012014).

Jiajie Guo and Wuguang Liu are with the State Key Lab. of Digital Manufacturing Equipment and Technology, Sch. of Mech. Sci. and Eng., Huazhong Univ. of Sci. and Tech., Wuhan, Hubei, 430074, P.R.China.

Kok-Meng Lee is with the Woodruff Sch. of Mech. Eng. at Georgia Inst. of Tech., Atlanta, GA 30332-0405 USA. He is also Distinguished Professor (National 1000 Talent Recruitment Plan) of Huazhong Univ. of Sci. and Tech.

* Corresponding author, 404-894-7402; kokmeng.lee@me.gatech.edu.

The remainder of this paper is organized as follows:

- Robot design concepts for obstacle avoidance are developed and analyzed from three aspects of dimension, attachment and flexibility, based on which an FMN is designed with a compliant beam and fixed arc magnet configuration.
- With the application of SHM [6, 18, 19] in mind, typical structural obstacles are considered as combinations of two basic corner types, and corresponding avoidance strategies are developed.
- To validate the proposed navigation strategy, both experiment and simulation are carried out for the FMN and the matched result suggests a simple displacement control for structural obstacle avoidance.

II. Design Concepts

Fig. 1 shows a network of autonomous robots, which are capable of carrying smart sensors and navigating on civil structures for health monitoring. Each robot is featured with small size, magnetic attachment and compliant mechatronics. Its front axle and rear axle are connected by a compliant beam, through which it can load/unload a sensor on the working surface and negotiate corners with various poses, so it is named as the flexonic mobile node (FMN).

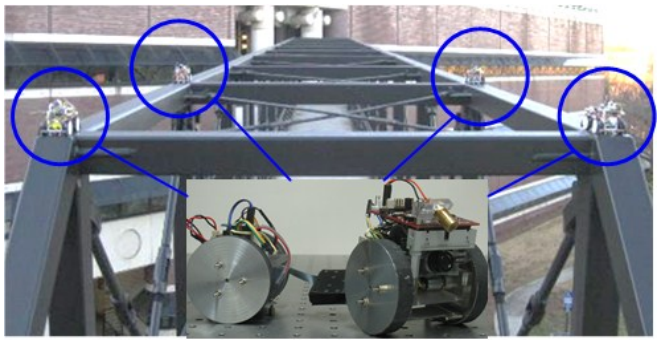

Fig. 1. Flexonic mobile node for SHM [19, 20].

As civil structures are built with established engineering criterions and standards, a field robot to navigate on these structures should be designed under certain guidelines, which can be categorized into the following topics of dimensions, attachment and flexibility. Along the discussion of these guidelines, the design concepts of the FMN are also delivered.

A. Dimension

Dimension of a field robot is obviously critical to its design of mechanical and electrical components. However, it is even more important to the function of obstacle avoidance. Fig. 2 shows a schematic of a general robot (either wheeled or legged) to overcome an obstacle, where the featured dimensions of the robot and the obstacle are denoted as R and H, respectively. In this way, the robot can be considered as a sphere of radius R, and it is subjected to a virtual pushing force F from motors or actuators. When the force can provide enough positive torque $F(R-H)$, the robot can overcome the obstacle. In this way, if R is much larger than H, it is very easy to climb the step as shown in Fig. 2(a). However, if R is close to H, or in other words, the robot is about the same size as an obstacle, it tends to be trapped as shown in Fig. 2(b). Also, if R is much smaller than H, then the task can be divided into a sequence of typical obstacle avoidance motions, such as negotiating concave and convex corners in Fig. 2(c). Of course, an attaching force would be required for certain motions, such as climbing, to compensate for the gravity.

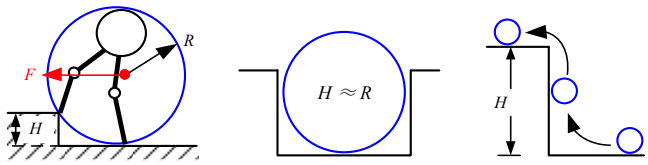

(a) Large (b) Medium (c) Small

Fig. 2. Robot dimension compared to obstacles.

With typical obstacles in mind, it is reasonable to design a robot either much larger or much smaller than the featured dimension of the obstacles. For SHM, an extremely big robot would be too heavy, energy inefficient and risky. Since the width and length of general trusses is larger than 15cm and 200cm, one axle of the FMN is designed as compact as about 8cm×8cm×8cm. In this way, navigation on complicated truss structures can be achieved with strategies developed for overcoming simple obstacles.

B. Attachment

Permanent magnets are employed to provide attraction forces to attach the FMN onto an iron surface. The novel concept of the fixed magnet configuration is developed from the general design of alternative rotating magnets. Fig. 3(a) shows one of the traditional magnetic wheels, where thin rectangular magnets envelop a solid cylinder with their magnetization axes arranged alternatively pointing towards and outwards from the wheel center. However, the new configuration fixes the magnet on the frame (Fig. 3b), so that the robot moves with the externally rotating wheel by only compensating for the friction; while in the design of rotating magnets, the wheel embodies a polygon profile and the driving force has to compensate for the magnetic force, which is much larger than the friction. As the polygon wheel moves on a surface, its center vibrates vertically because of the varying rotation radius. This dynamics contributes to the tilting of the robot frame body (Fig. 3b), which deteriorates the performance of the onboard sensors such as the image processing unit. In this way, the supporting columns have to be added to maintain the frame orientation. But the fixed magnet configuration can naturally maintain its pose in a similar manner as a tumbler, thus can perform much smoother motions.

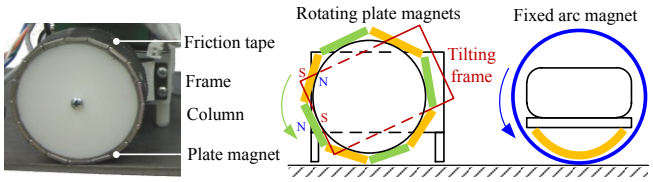

(a) Traditional design of a magnetic wheel.

(b) Comparison of rotating and fixed magnet configurations.

Fig. 3. Comparison of two magnetic wheel configurations.

By realizing the concept of fixed magnet configuration, Fig. 4 shows the mechanical structure of the FMN. Two arc magnets, which are radially magnetized in the opposite directions, are fixed with the frame body through the guards (radius is 30 mm). Each of the hollow wheels (inner and outer radii are 31 mm and 32.5 mm, respectively) is independently driven by one DC motor. As a magnetic force decreases dramatically with distance, the gap between the magnets and the surface is designed to be about 3.5 mm. Also, an iron plate is added to increase the wheel attraction force by forming a closed-loop of magnetic flux. After assembled with the electronic components, the overall weight of one axle is measured as about 0.4 kg, which is mainly contributed by the motors, batteries and magnets as main parts of the FMN are made of Delrin.. So a robot design with the fixed magnet configuration is anticipated to be lighter than that using many magnets in the traditional configuration.

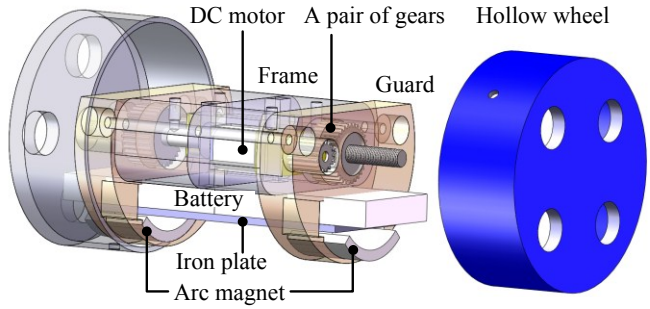

(a) CAD model.

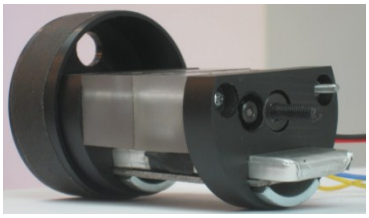

(b) Mechanical structure.

Fig. 4. Mechanical parts of the FMN.

C. Flexibility

A field robot is desired to be as flexible as possible to negotiate various types of obstacles, implying the more degrees of freedom (DOFs) the better. A four-wheel robot is used as a comparison platform for different design configurations. Assuming the robot is self-balanced with fixed magnets as proposed in the previous section, the rear axle embodies 2 DOFs as it can move forward/backward and make turns on a plane. In the following, the front axle relative motion is analyzed for four design configurations and their total DOFs are summarized in Table I:

- *DC1 (Link)*: When connected with a rigid link, the front axle has no relative motion to the rear axles.
- *DC2 (Pin joint)*: The added pin joint allows the front axle to rotate with respect to the rear axle. The rotation direction depends on the pin axis orientation.
- *DC3 (Ball joint)*: The front axle is able to rotate in the 3D space with a ball joint characterized by yawing, pitching and rolling. However, the rotation range is limited, and the distance between the two axles is uniquely determined once the front axle orientation is known.
- *DC4 (Compliant beam)*: By connecting with a compliant beam subject to both bending and twisting, the front axle is capable of both rotation and translation in the 3D space, and the rotation range is much larger than DC3. It is noted that the compliant beam can have infinite number of deformed shapes, which has not been accounted in this analysis.

TABLE I
COMPARISON OF DEGREES OF FREEDOM

DC 1	DC 2	DC 3	DC 4
Front / Rear			
DOF = 2	DOF = 3	DOF = 5	DOF = 8

III. OBSTACLE AVOIDANCE

With typical engineering components in mind, geometries of most structural obstacles are combinations of different surfaces. So obstacle avoidance of an FMN can be achieved by navigating from one plane to another. This can be decoupled into two basic strategies of corner negotiation.

A. Convex Corner

Fig. 5 shows an FMN crossing a convex corner A from plane I to plane II. The reference frame XYZ is defined such that axis Z is normal to the plane I where the FMN initially locates and axis X is normal to the corner edge. Similarly, the frame X′Y′Z′ is obtained by rotating the frame XYZ with respect to the axis Y so that Z′ is normal to the plane II. Because of limited turning space, the FMN changes its initially aligned front and rear axles by turning the front axle (equivalent to a rigid body with mass m_1 and mass center C_1, and the wheel radius is r_w) and deforming the compliant beam. Coordinate frames $P_0x_0y_0z_0$ and $P_1x_1y_1z_1$ are attached to the beam rear and front ends, where x_0 and x_1 are along the beam axis while z_0 and z_1 are normal to the beam surface, so they characterize positions and orientations of both ends, respectively.

The strategy for the FMN to negotiate a convex corner with limited turning space comprises three steps:

Step 1: The rear axle turns so that the front axle can approach the edge perpendicularly, where β is the angle between X and x_0. Afterwards the rear axle pushes forwards by u_0 along x_0, exerting forces $\boldsymbol{F}_1$ and torque $\boldsymbol{M}_1$ through the compliant beam to rotate the front axle about A by α which is determined by the angle formed by the axes Z and z_1.

Step 2: Right after the front axle crosses over the corner, the two axle move together.

Step 3: As soon as the rear axle reaches the corner, it is pulled over by the front axle via the compliant beam.

Step 1 is detailed in the following as the success of the convex corner negotiation in the 3D space is dictated by this initiation, which differs from the 2D case as presented in previous research [6]. In Fig. 5, N is the normal force acting on both wheels of the front axle; $f\,(=\mu N)$ is the friction; μ is the coefficient of friction between the wheel and the ground; and M_{m} is the torque provided by the front axle motors. The following assumptions are made in this discussion:

1) The magnetic wheels are designed as in Section IIB so that the FMN is attached on the steel surfaces as it moves.

2) The non-slip condition is satisfied:

$$M_m = f r_w \le \mu N(\alpha) r_w . \tag{1}$$

3) Because the magnets are very close to the surface, the moment arm is very small, thus the magnetic torque is negligible as compared to that due to gravity.

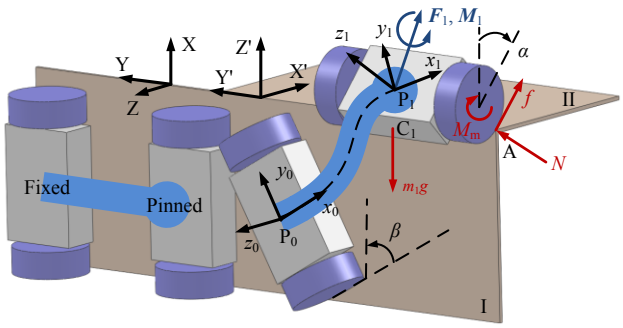

Fig. 5. Turning with limited space.

For the front assembly to cross the corner, the inequality (2) must be satisfied with respect to A:

$$\left| M_r \mathbf{i}_Y + \mathbf{r}_{C_1} \times m_1 \mathbf{g} \right| \ge 0 \tag{2}$$

where $M_r \mathbf{i}_Y = -\mathbf{r}_{P_1} \times \mathbf{F}_1 - \mathbf{M}_1$ is the required moment to compensate for the gravitational torque, $\mathbf{i}_{\mathrm{Y}}$ is a unit vector along the Y axis, $\mathbf{r}_{C_1}$ and $\mathbf{r}_{P_1}$ are the projected arm lengths of AC_1 and AP_1 on the plane XZ. The boundary conditions for negotiating a convex corner can be obtained from (3) and (4):

$$\mathbf{M}_1 = \mathbf{r}_{C_1} \times m_1 \mathbf{g} - \mathbf{r}_{P_1} \times \mathbf{F}_1 \tag{3}$$

$$\left[x_1\ y_1\ z_1\right]^{\mathrm{T}} = \left[L\ 0\ 0\right]^{\mathrm{T}} + \left[\mathbf{R}_\beta\right]\left(\left[\mathbf{R}_\alpha\right]^{\mathrm{T}} - \left[\mathbf{I}\right]\right)\mathbf{r}_{P1} \tag{4}$$

where $\left[\mathbf{R}_\alpha\right] = \begin{bmatrix} \cos\alpha & 0 & -\sin\alpha \\ 0 & 1 & 0 \\ \sin\alpha & 0 & \cos\alpha \end{bmatrix}$, $\left[\mathbf{R}_\beta\right] = \begin{bmatrix} \cos\beta & -\sin\beta & 0 \\ \sin\beta & \cos\beta & 0 \\ 0 & 0 & 1 \end{bmatrix}$

and L is the initial beam length. It is noted that the above equations are formulated in vector forms, so they are valid for any direction the FMN moves towards relative to the gravity.

Motions of the FMN can be simulated by solving the 3D compliant beam governing equations (Appendix) with boundary conditions provided by (3) and (4). Fig. 6 illustrates a snapshot of the beam deformation (both bending and twisting) for the pushing angle $\beta = 60°$, where rotation of the front axle can be obtained from the rotation of the beam end $P_1x_1y_1z_1$ projected on the surface XZ as $\alpha = 27°$.

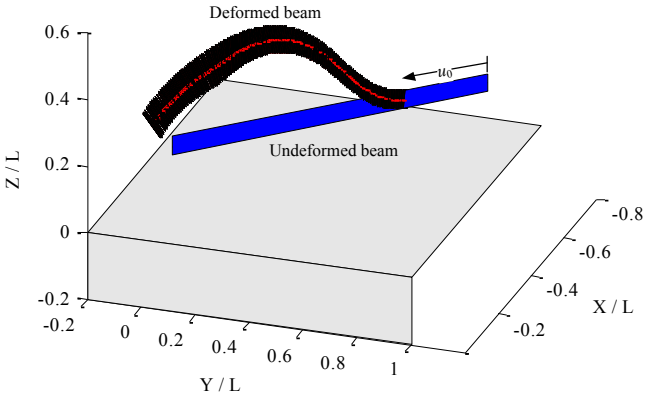

Fig. 6. Simulation of a compliant beam ($\alpha = 27°, \beta = 60°$).

B. Concave Corner

Compared to the 3-step strategy to negotiate convex corners with limited space, concave corner negotiation is much simpler because it is automated in nature by the fixed magnet configuration as illustrated in Fig. 7. Considering only one axle approaching the corner on the plane I, it is driven by the motor torque M_{m} as given by (1). Once the wheels push against the plane II, the axle could not move any further and the wheels get stuck (Fig. 7a). As the wheels do not rotate, the frame would be subjected to the reaction torque from the wheels, which is equal to $-M_{\mathrm{m}}$. Although the magnetic forces are very large to attach the robot to any iron surface, the magnetic torque is actually smaller than the motor torque, thus the frame starts to rotate as shown in Fig. 7b. After the magnets get released from the plane I and attracted to the plane II, the axle can continue moving and the task of concave corner negotiation is achieved.

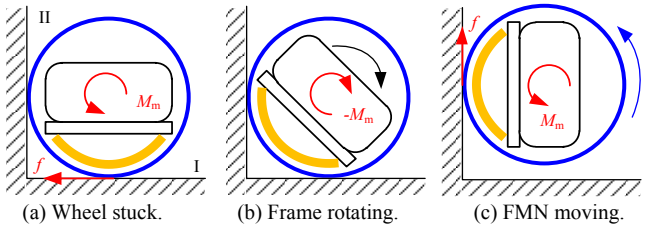

(a) Wheel stuck. (b) Frame rotating. (c) FMN moving.

Fig. 7. Concave corner negotiation.

IV. Experiment and Results

The proposed design concepts of FMN are realized as shown in Fig. 8. One end of the beam is rigidly fixed on the rear axle frame while the other end is pinned and coupled with a slider. As the pin moves to the right end (Fig. 8a), the beam

front edge pushes against the front axle and is locked as fixation. When the pin is at the other end, there is a gap between the beam front edge and back of the front axle, allowing for free rotation between them and facilitating in-plane turning without twisting the beam. Besides, electronic components of image processing and wireless communication are also implemented on the FMN prototype for application of SHM.

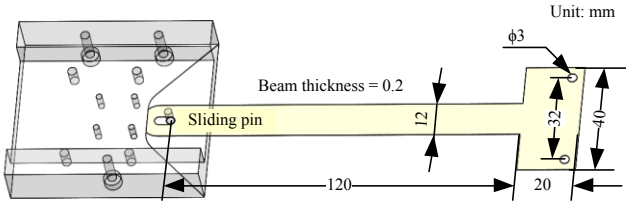

(a) Compliant beam design with a sliding pin.
(Spring steel: E = 207 GPa; v = 0.3; density = 7.63 g/cm^3).

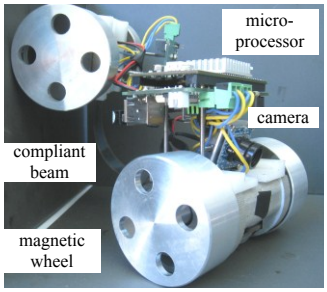

(b) FMN mechatronics.

Fig. 8. Prototype of the FMN.

The objectives of the experiment are as follows:

1) The first objective is to validate the proposed obstacle avoidance strategy for convex corner negotiation, where the pushing angle varies from 0º to 60º.
2) The second is to validate the theoretical model for corner negotiation based on a compliant beam by comparing simulation result against experiment.
3) The third is to find a control method potentially effective to obstacle avoidance. Of particular interest is to determine the rear axle displacement u_0 for a desired front axle rotation angle α.

Fig. 9 shows the experiment setup for the front axle to overcome a right corner on a steel structure. To accurately maintain the pushing angle β and measure the rear axle displacement u_0, the rear axle is replaced by a set of manual positioners. The translation stages in Part A are used to adjust the height of the compliant beam to obtain a horizontal initial state, while those in Part B measure the pushing displacement u_0 from 0 to 75mm. The rotation stage in Part C is employed to manipulate β, thus can change the direction of the complaint beam relative to the front axle.

Snapshots of the front axle wheel are captured by a digital camera for each value of u_0 as shown in Fig. 10(a), and the wheel center is calculated by image processing techniques. Then, the rotation angle α of the front axle is obtained by the orientation of the line connecting the wheel center and the corner point. Since the simulation results for different β are very close to each other, average of the simulation result is compared against the cases of β increased from 0º to 60º with increment of 15º in Fig. 10(b). It is shown that simulation closely matches with the experiment results, although deviations exist for β = 0º and 30º. It is noted that errors may come from calculation of the required torque that involves determination of the assembly mass center. Another error source would be the image processing when the corner point is determined by manually picking one pixel, which gives rise to negative initial value of α. Besides, it is obvious that the rotation angle α is linear with the rear axle displacement u_0 for different pushing angle β, which potentially facilitate the control implementation for corner negotiation.

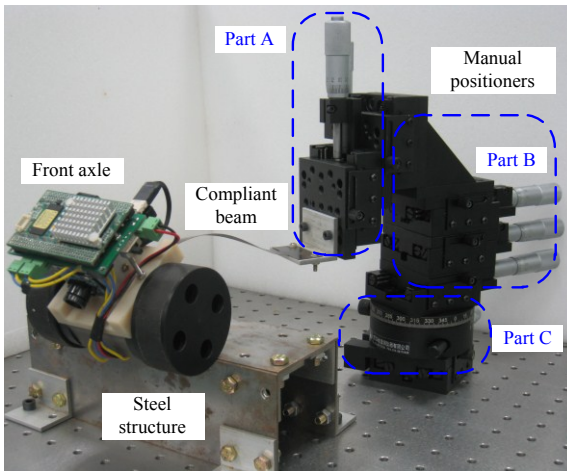

Fig. 9. Experimental setup.

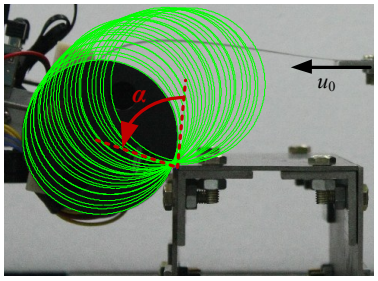

(a) Detection of front axle rotation.

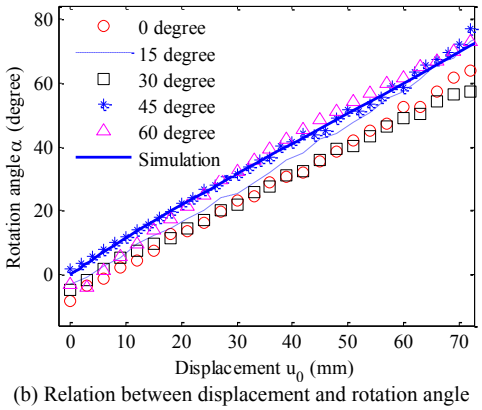

(b) Relation between displacement and rotation angle

Fig. 10. Experiment result.

V. Conclusion

Motivated by the application of structural health monitoring (SHM), this paper has proposed a flexonic mobile node (FMN) based on several design concepts from three aspects of dimension, attachment and flexibility. To facilitate structural obstacle avoidance, the dimension of the robot should be either much larger or much smaller than the targeted obstacles. A novel magnetic wheel configuration is developed by fixing arc magnets to the robot frame, which performs smoother motion than traditional design with rotating magnets. Also, this fixed magnet configuration is able to maintain the robot frame orientation and automate the concave corner negotiation. For the case of convex corner negotiation, a 3-step strategy is presented by incorporating a compliant beam (embodies more DOFs than links and pin/ball joints) , where both simulation and experiment results confirm a linear relation between the front axle rotation and rear axle displacement. As typical structural elements can be decoupled into convex and concave corners, the method developed in this paper can be readily used for structural obstacle avoidance.

Appendix

In Fig. A, the local coordinate frames "$x_s y_s z_s$" (each with a subscript $0 \le s/L \le 1$ as the path length describing its location along the beam axis, L is the beam length) are defined in such a way that x_s is along the neutral axis of the beam, and z_s is normal to the beam surface. Then the coordinate $[x_s\ y_s\ z_s]^T$ for the material point P_s describes the beam shape with respect to the reference frame $P_0x_0y_0z_0$.

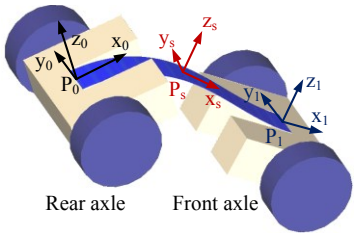

Fig. A. Coordinate frames for a FMN.

The governing equations for a 3D compliant beam are given as

$$\mathbf{R}_i' = k_3\mathbf{R}_2 - k_2\mathbf{R}_3 \tag{A1}$$

$$\varphi' = k_1 - k_2\frac{R_{12}C\varphi + R_{13}S\varphi}{1+R_{11}} - k_3\frac{R_{13}C\varphi - R_{12}S\varphi}{1+R_{11}} \tag{A2}$$

$$\mathbf{x}' = (1+\varepsilon)\mathbf{R}_1 \tag{A3}$$

$$\mathbf{F}' = -\mathbf{q}_F \tag{A4}$$

$$\mathbf{M}' = -\mathbf{q}_M - [(1+\varepsilon)\mathbf{e}_1]\times\mathbf{F} \tag{A5}$$

where the prime denotes derivative with respect to s; $\mathbf{R}_i$ (i = 1, 2 and 3) is the i^{th} row of the rotational matrix $[\mathbf{R}]$ between the frames $P_0x_0y_0z_0$ and $P_sx_sy_sz_s$; φ is the twisting angle, with $C\varphi = \cos\varphi$, $S\varphi = \sin\varphi$; $\mathbf{x} = [x_s\ y_s\ z_s]^T$ is the nodal coordinate; $\mathbf{F} = [F_1\ F_2\ F_3]^T$ and $\mathbf{M} = [M_1\ M_2\ M_3]^T$ are the nodal force and moment; $\mathbf{q}_F$ and $\mathbf{q}_M$ are the distributed force and moment, respectively.

Strain ε and curvature $\mathbf{K} = [k_1\ k_2\ k_3]^T$ are given by:

$$\varepsilon = (F_1R_{11} + F_2R_{12} + F_3R_{13})/(EA) \tag{A6}$$

$$k_i = k_i^{(0)} + \mathbf{M}\cdot\mathbf{R}_i/(GI_i) \tag{A7}$$

where E is the Young's modulus, G is the shear modulus; I_i (i = 1, 2 and 3) is the moment of inertia, A is the cross-sectional area; and $\mathbf{K}^{(0)} = \left[k_1^{(0)}\quad k_2^{(0)}\quad k_3^{(0)}\right]^T$ is the initial curvature. Detailed formulation can be found in [20].

References

[1] J. P. Lynch and K. J. Loh, "A summary review of wireless sensors and sensor networks for structural health monitoring," *Shock Vibration Dig.*, vol. 38, pp. 91-128, 2006.

[2] C. B. Yun and J. Min, "Smart sensing, monitoring, and damage detection for civil infrastructures," *KSCE Journal of Civil Engineering*, vol. 15, no. 1, pp. 1-14, 2011.

[3] Y. Y. Li and Y. Chen, "A review on recent development of vibration-based structural robust damage detection," *Structural Engineering and Mechanics*, vol. 45, no. 2, pp. 159-168, 2013.

[4] S. Chesne and A. Deraemaeker, "Damage localization using transmissibility functions: A critical review," *Mechanical Systems and Signal Processing*, vol. 38, no. 2, pp. 569-584, 2013.

[5] J. Guo and K.-M. Lee, "Compliant joint design and flexure finger dynamic analysis using an equivalent pin model," *Mechanism and Machine Theory*, vol. 70, pp. 338-353, 2013.

[6] J. Guo, K.-M. Lee, D. Zhu, X. Yi, and Y. Wang, "Large-deformation analysis and experimental validation of a flexure-based mobile sensor node," *IEEE/ASME Trans. on Mechatronics*, vol. 17, no. 4, pp. 606-616, 2012.

[7] J. Schultz and J. Ueda, "Two-port network models for compliant rhomboidal strain amplifiers," *IEEE Transactions on Robotics*, vol. 29, no. 1, pp. 42-54, 2013.

[8] Y. J. Park, U. Jeong, J. Lee, S. R. Kwon, H. Y. Kim, and K. J. Cho, "Kinematic condition for maximizing the thrust of a robotic fish using a compliant caudal fin," *IEEE Transactions on Robotics*, vol. 28, no. 6, pp. 1216-1227, 2012.

[9] D. B. Camarillo, C. R. Carlson, and J. K. Salisbury, "Configuration tracking for continuum manipulators with coupled tendon drive," *IEEE Transactions on Robotics*, vol. 25, no. 4, pp. 798-808, 2009.

[10] R. Pfeifer, M. Lungarella, and F. Iida, "Self-organization, embodiment, and biologically inspired robotics," *Science*, vol. 318, no. 5853, pp. 1088-1093, 2007.

[11] G. S. Chirikjian and J. W. Burdick, "The kinematics of hyper-redundant robot locomotion," *IEEE Trans. on Robotics and Automation*, vol. 11, no. 6, pp. 781-793, 1995.

[12] P. Liljeback, K. Y. Pettersen, O. Stavdahl, and J. T. Gravdahl, "Experimental investigation of fundamental properties of snake robot locomotion," in *Proc. 11th International Conference on Control Automation Robotics & Vision (ICARCV)*, Singapore, 2010, pp. 187-194.

[13] C. Stefanini, S. Orofino, L. Manfredi, S. Mintchev, S. Marrazza, T. Assaf, L. Capantini, E. Sinibaldi, S. Grillner, P. Wallen, and P. Dario, "A novel autonomous, bioinspired swimming robot developed by neuroscientists and bioengineers," *Bioinspiration & Biomimetics*, vol. 7, no. 2, 2012:025001.

[14] S. X. Guo, T. Fukuda, and K. Asaka, "A new type of fish-like underwater microrobot," *IEEE/ASME Trans. on Mechatronics*, vol. 8, no. 1, pp. 136-141, 2003.

[15] Z. Chen, S. Shatara, and X. B. Tan, "Modeling of biomimetic robotic fish propelled by an ionic polymer-metal composite caudal fin," *IEEE/ASME Trans. on Mechatronics*, vol. 15, no. 3, pp. 448-459, 2010.

[16] R. J. Webster and B. A. Jones, "Design and kinematic modeling of constant curvature continuum robots: A review," *Int. J. of Robotics Research*, vol. 29, no. 13, pp. 1661-1683, 2010.

[17] R. J. Webster, J. M. Romano, and N. J. Cowan, "Mechanics of precurved-tube continuum robots," *IEEE Trans. on Robotics*, vol. 25, no. 1, pp. 67-78, 2009.

[18] K.-M. Lee, Y. Wang, D. Zhu, J. Guo, and X. Yi, "Flexure-based mechatronic mobile sensors for structure damage detection," presented at the 7th International Workshop on Structural Health Monitoring, Stanford CA, USA, 2009.

[19] D. Zhu, J. Guo, C. H. Cho, Y. Wang, and K.-M. Lee, "Wireless mobile sensor network for the system identification of a space frame bridge," *IEEE/ASME Transactions on Mechatronics*, vol. 17, no. 3, pp. 499-507, 2012.

[20] J. Guo, Y. Xie, and K.-M. Lee, "Three-dimensional large deformation of a compliant beam designed for a flexonic mobile node," in *Proceedings of the ASME Dynamic Systems and Control Conference*, Arlington, VA, USA, 2012, vol. 2, pp. 159-165.